International Journal of Machine Tools & Manufacture 84 (2014) 9–16

Contents lists available at ScienceDirect

International Journal of Machine Tools & Manufacture

journal homepage: www.elsevier.com/locate/ijmactool

Finite element and experimental studies of the formation mechanism of edge defects during machining of SiCp/Al composites

L. Zhou [a], Y. Wang [a], Z.Y. Ma [b,*], X.L. Yu [a]

[a] School of Mechanical Engineering, Shenyang Ligong University, Shenyang 110159, China
[b] Institute of Metal Research, Chinese Academy of Sciences, Shenyang 110016, China

ARTICLE INFO

Article history:
Received 25 October 2013
Received in revised form
10 March 2014
Accepted 14 March 2014
Available online 19 April 2014

Keywords:
SiCp/Al composites
Formation mechanism
Edge defects
Orthogonal cutting experiment
Finite element

ABSTRACT

In this paper, a multi-particle microfinite element model with a random particle distribution in SiCp/Al composites was developed using ABAQUS software. The formation mechanism of edge defects near the exit of orthogonal cutting was analyzed, and the effects of cutting parameters on the sizes of edge defects were investigated. The results indicate that both the brittle fracture of SiC particles and the plastic flow of Al matrix occur in the process of the edge defects formation. Additionally, the cutting speed has little effect on the sizes of edge defects but the cutting depth has a significant effect on the height and length of edge defects. The numerical results were also compared to the orthogonal cutting experimental data and found to be in reasonable agreement.

1. Introduction

SiCp/Al composites have become very promising materials due to their significant advantages over conventional material such as high specific modulus, high specific strength, low coefficient of thermal expansion, excellent fatigue resistance and corrosion resistance, and therefore are increasingly used in automotive and aerospace structures [1–4]. Especially, SiCp/Al composites with high reinforcement volume fractions (> 50 vol%) are often used for thermal management applications such as electronic packaging. Since the mechanical properties of SiC particles are completely different from those of the Al alloy matrix, the deformation and fracture models of SiC particles are also very different from those of the Al matrix during machining of SiCp/Al composites. It is well known that burrs are formed easily as the result of the plastic flow from cutting and shearing operations when machining ductile materials. On the contrary, for brittle materials a negative deformation plane will be initiated when the steady-state chip formation stops as the tool approaches the end of the cut and the edge breakout occurs instead of burr formation [5]. In a broader sense, the edge defects are defined as undesirable or unwanted projections generated at the edge of the components after the machining process. The presence of these edge defects not only has passive effect on the dimensional tolerances, position accuracy and the assembly process of the product, but also reduces the product durability and service life.

In the past decades, many experimental and simulation studies have been used extensively to investigate the burr formation, control and deburring. Toropov et al. [6,7] conducted turning experiments to investigate the burr formation in connection with tool angles and workpiece angles, as well as cutting conditions, and proposed a model of the burr formation mechanism when burrs are formed in the feed direction during turning operation. In turning operations, most burrs are created as a rollover burr at the side of the workpiece when the tool exits from cutting [8]. Chern [5,9] studied the burr formation and edge breakout on the workpiece exit edge in orthogonal cutting and face milling of aluminum alloys. Olvera and Barow [10] investigated the influence of the main cutting parameters on the burr formation in square shoulder face milling operation. Exit burr in the cutting direction, exit burr in the feed direction and burr formed at the top edge were discussed through their extensive experimental research. More generally, drilling is an important final machining process for joining and assembling. Therefore, there are many research papers devoted to the study of the burr formation in drilling operation [11–14]. After a basic understanding of the burr formation mechanisms has been reached, the focus of research turned to the deburring techniques and how to control or minimize the burr size. Deburring is a very difficult engineering problem and, until now, there are many deburring methods which have been developed, such as mechanical deburring [15], thermal energy deburring [16], electrochemical deburring [17,18], ultrasonic deburring [19], etc. Besides, edge chipping is one of the typical edge damage modes

* Corresponding author. Tel./fax: +86 24 83978908.
E-mail address: zyma@imr.ac.cn (Z.Y. Ma).

http://dx.doi.org/10.1016/j.ijmachtools.2014.03.003
0890-6955/© 2014 Elsevier Ltd. All rights reserved.

in machining ceramic materials. The forming mechanism [20,21], reducing [22] and preventing edge chipping [23] were investigated by experimental and simulation methods. Finite element method can be used as a tool to understand and predict burr or edge chipping formation, and most of the work carried out so far is on the machining of isotropic materials. Park and Dornfeld [24,25] have modeled burr formation process and investigated the influences of various process parameters in two-dimensional orthogonal cutting of AISI 304 stainless steel. Guo and Dornfeld [26] developed a three-dimensional finite element model for modeling drilling and exit burr formation. Cao [27] studied the factors related to exit edge chipping in milling of ceramics using a two-dimensional finite element model.

It is clear that the presence of reinforcement makes metal matrix composites (MMCs) different from monolithic materials due to incorporation of superior physical properties into the MMC [12]. Therefore, the formation mechanism of edge defects during machining of SiCp/Al composites is expected to be different from that of homogeneous metal or brittle material. Although numerous reports can be found in the literature describing the experimental studies related to the delamination during drilling of carbon fiber reinforced plastics composites [13,28,29], and little research on the formation mechanism of edge defects in machining of SiCp/Al composites, especially using the microfinite element method.

In this paper, a microfinite element model was developed using commercial software (ABAQUS/Explicit) to analyze the formation mechanism of edge defects during machining SiCp/Al composites. Additional, the numerical results were also compared to the orthogonal cutting experiments at different cutting depths and speeds in order to investigate the effects of various cutting parameters on the edge defects size.

2. Experimental procedures

The orthogonal cutting experiments were conducted on SiCp/Al composites, in which the volume fraction is 56% and the average edge size is about 60 μm for SiC particles, as shown in Fig. 1. The physical and mechanical properties of SiCp/Al composites are listed in Table 1. The size of experimental samples was prepared in the form of $59 \times 47 \times 4\ mm^3$ by cutting in a wire electrical discharge machine.

The experimental setup is schematically illustrated in Fig. 2. It mainly consists of a spindle system and a data acquisition system. All the cutting tests were performed on a high-precision vertical machining center EUMA ME650. The summary of experimental conditions is listed in Table 2. Four undeformed chip thickness 0.05, 0.1, 0.15 and 0.2 mm, five cutting speeds 1, 3, 5, 7 and 9 m/min and a fixed cutting width of 4 mm were used as cutting conditions. The cutting tests were performed with polycrystal diamond (PCD) tool, and the PCD insert has the grain size of 25 μm. The tool rake angle was $\gamma^0 = 0^\circ$, and the clearance angle was $\alpha = 8^\circ$. During experiments, only one of the parameters, such as the cutting speed was varied while the cutting depth was held constant to observe the effect of individual parameter on the exit edge defects. After testing, the fracture morphology and the size of edge defects were viewed by scanning electron microscopy (SEM) and a digital optical microscope (KEYENCE, VHX-1000), respectively.

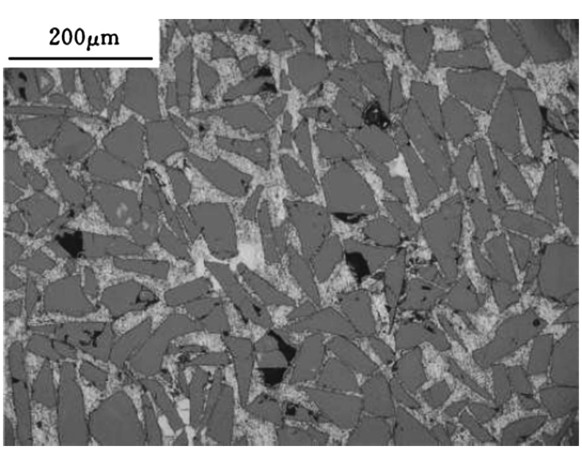

Fig. 1. Microstructure of the SiCp/Al composites.

Table 1
Physical and mechanical properties of SiCp/Al composites.

Properties	Value
Density (g/cm^3)	2.94
Elastic modulus (GPa)	220
Flexure strength (MPa)	405
Hardness (HV: N/mm^2)	200
Coefficient of thermal expansion (10^{-6}/K)	8.0

3. Finite element modeling procedure

3.1. Finite element model

In order to investigate the effect of SiC particles on the formation mechanism of edge defects during machining of SiCp/Al composites, a two-dimensional plane strain and random distribution multi-particle micro-model was constructed using ABAQUS/Explicit version 6.11.3, as shown in Fig. 3. The particle size and volume fraction are the same with those of the experiment. In this model, the matrix and the particles are identified independently and the four-node plane strain bilinear quadrilateral elements (CPE4RT) with reduced integration and hourglass control were used to mesh the particles and matrix. To confirm mesh size convergence in this model, test simulations with varying mesh sizes were conducted at a cutting speed of 5 m/min and depth of 0.1 mm, and a comparison was made between the simulated and experimental measurements of the cutting force. The global element size is reduced in descending order of 0.012, 0.008, and 0.005 mm, corresponding to this the normalized cutting force is 263, 277 and 285 N, respectively. The best element size set until a reasonable match (about 10% error) in simulated and measured cutting forces is achieved, and a minimum element size of 0.005 was finally selected for all other cutting conditions. Therefore, the setting of the global element size is a good balance of the computation time and the required accuracy. The particles were assumed to be perfectly bonded with the matrix, and the interface nodes of the matrix and particles were tied together. In order to show the mesh clearly, the upper left corner in Fig. 3a has been amplified as shown in Fig. 3b.

3.2. Materials constitutive equation

Although a multi-particle cell model presented by Zahr Vinuela and Pérez Castellanos [30] shown that Halpin–Tsai equation is one of the most effective equations in predicting the mechanical behavior for paticulate reinforced metal matrix composites. In this paper, in order to observe the internal stress distributions both for the matrix and SiC particles during the cutting process, the constitutive equations of Al alloy and SiC particle were defined, respectively. It is well known that the flow behavior of Al alloy is

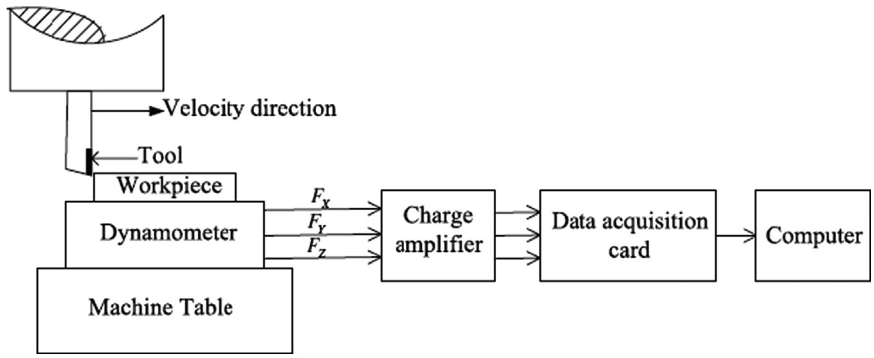

Fig. 2. Illustration of experimental setup.

Table 2
Summary of experimental conditions.

Machine	EUMA ME650 vertical machining center
Tool	Polycrystal diamond (PCD) tool, grain size, 25 μm, rake angle γ^0, 0°, clearance angle α, 8°.
Workpiece materials	56 vol.% SiCp/Al composites
Cutting speed (m/min)	1, 3, 5, 7, 9
Cutting depth (mm)	0.05, 0.1, 0.15, 0.2
Cutting conditions	Dry

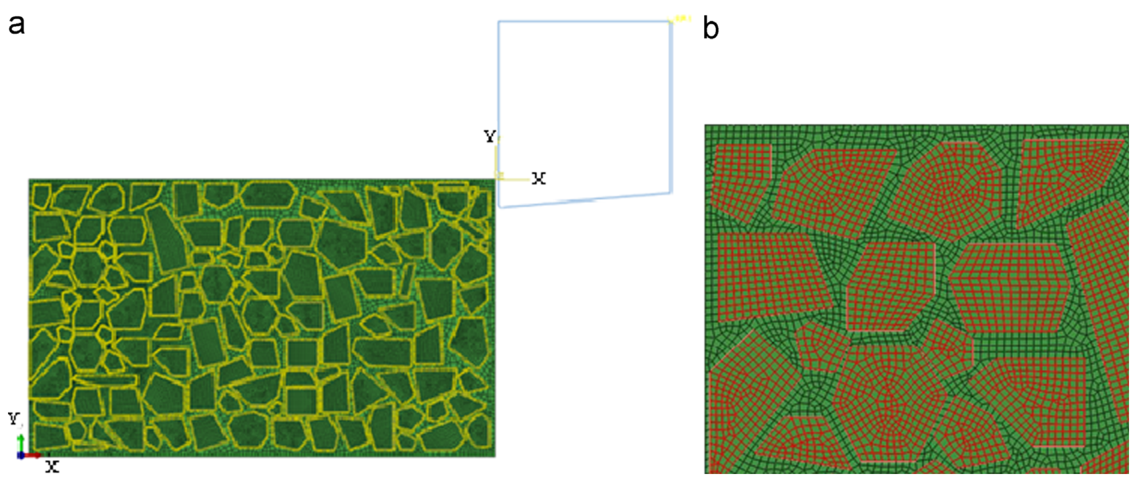

Fig. 3. (a) Finite element model of orthogonal cutting of SiCp/Al composites and (b) local zooming of (a).

Table 3
Material constants of Al alloy [31].

A (MPa)	B (MPa)	C	n	m
265	426	0.001	0.183	0.859

strongly dependent on the strain rate and temperature, and Johnson–Cook constitutive equation can provide a good description of the metal material behavior, subjected to large strain, strain rate and high temperature. Therefore, the Johnson–Cook constitutive equation was employed for Al alloy, which can be represented by the following:

$$\sigma = (A + B\varepsilon^n)\left[1 + C\ln\frac{\dot{\varepsilon}}{\dot{\varepsilon}_0}\right]\left[1 - \left(\frac{T - T_0}{T_{melt} - T_0}\right)^m\right] \tag{1}$$

where σ is the flow stress, ε is the plastic strain, $\dot{\varepsilon}$ is the strain rate, $\dot{\varepsilon}_0$ is the reference plastic strain rate, T is the workpiece temperature, and T_{melt} and T_0 are the material melting and room temperature, respectively. Coefficient A is the yield strength, B is the hardening modulus, C is the strain rate sensitivity coefficient, n is the hardening coefficient, and m is the thermal softening coefficient. The material constants of Al alloy matrix are obtained from literature as shown in Table 3. Additionally, the SiC particles are modeled as an isotropic perfectly elastic material following the generalized Hook's law. Since the interface is very hard and brittle and hence similar to the particles [31], the interface was

Table 4
Mechanical properties applied in the finite element computational analysis [31,32].

Material properties	Al alloy matrix	SiC particles	PCD tools
E, Young's modulus (GPa)	70.6	420	1.147
ν, Poisson's ratio	0.34	0.14	0.07
Coefficient of thermal expansion (K^{-1})	23.6×10^{-6}	4.9×10^{-6}	4.0×10^{-6}
ρ, Density (kg m^{-1})	2.7×103	3.13×103	4.25×103
k, Thermal conductivity (W m^{-1} K^{-1})	180	81	2100
CP, specific heat (J kg^{-1} K^{-1})	880	427	525

considered as an extension of the particle, and the SiC particles were assumed to be perfectly bonded with the Al alloy matrix. The cutting tool was treated as a rigid body. The material parameters applied in the finite element computational analysis are listed in Table 4. The units of the modeling process were: s, mm, MPa, N, and mm/s.

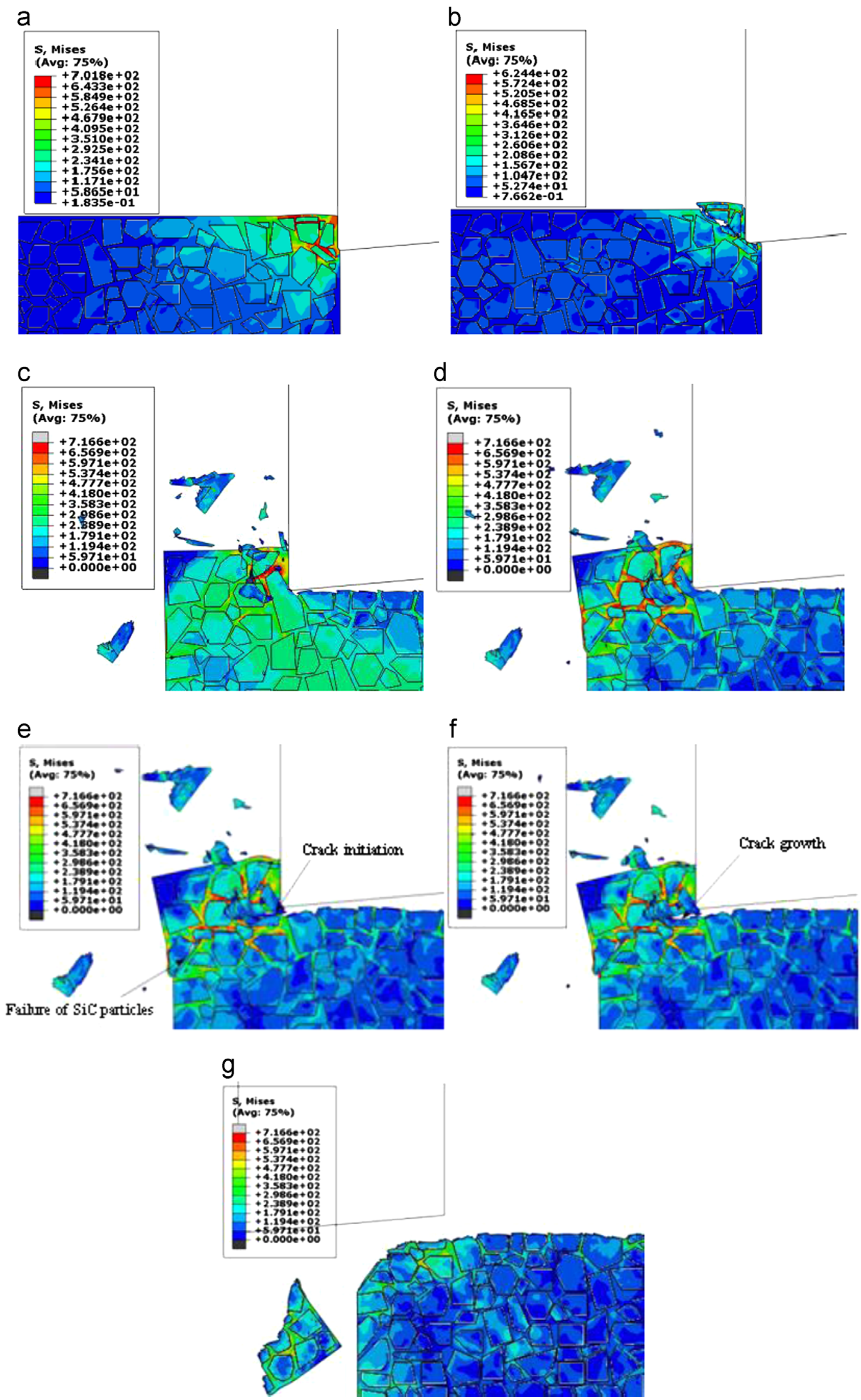

Fig. 4. Formation process of the edge defects during machining of SiCp/Al composites.

3.3. Chip separation criterion

For Al alloy matrix, the physical chip separation criterion available with ABAQUS/Explicit was used. According to the physical criterion, chip separation occurs when the strain value of the leading node is greater than or equal to a given value. The chip separation developed in the study was based on the shear failure mode using the shear failure module. The shear failure module is based on the equivalent plastic strain, ε. When an element of the matrix mesh reaches the damage plastic strain value ε^d, the damage parameter D in Eq. (2) equals to one. When this occurs, the material fails, and the corresponding element will be deleted.

$$D = \frac{\varepsilon}{\varepsilon^d} = 1 \tag{2}$$

In addition, for a SiC element, the failure will initiate in a brittle fracture mode when the maximum stress satisfies the failure criterion. More generally, the two stress failure criteria used are the maximum normal stress criterion and von Mises stress criterion. In this simulation, the maximum normal stress criterion was adopted for SiC particles; the crack is assumed to initiate if $\sigma \geq \sigma_{ut}$, where σ is the maximum principal stress obtained from the finite element simulation, and σ_{ut} is the tensile strength of the SiC particles. Moreover, the adaptive meshing technique was also incorporated to the pure deformation technique in the chip formation modeling process.

3.4. Boundary conditions and loads

In this model, the SiC particles were assumed to be perfectly bonded with the Al alloy matrix, and the interface nodes of the matrix and particles were tied together, therefore the initial displacements at the interface are equal for both the matrix and particles. In addition, the workpiece was constrained against movement in any direction at the bottom.

The tool was treated as a rigid body and moved horizontally into the workpiece at a predetermined speed with a constant cutting thick; to avoid the tool rotational and translational movement in the vertical direction, constraints were input on the reference node in this direction.

During the chip formation, two contact zones occur between tool and workpiece. The first contact is between the tool rake face and the produced chip, and the second contact is between the tool flank face and the generated surface. In this study, due to the low cutting speed and cutting depth, and the high volume fraction of SiC particles in the composites, the cutting temperature is not high and segmented chips are formed during the cutting process. Thus, the occurring of sticking zone at the tool–chip interface is not obvious and the relative sliding of chip on the rake surface occurs more easily. In the Coulomb friction law, the frictional stress (τ) is proportional to the normal stress (σ_n) with a friction coefficient (μ) as in ($\tau = \mu\sigma_n$).Therefore, these two contacts were assumed in this model to be controlled by the Coulomb friction law, and a constant Coulomb friction coefficient of $\mu = 0.5$ is used in all simulations since it represents sliding contact condition between the tool and the workpiece.

4. Results and discussions

4.1. Formation process of edge defects

Fig. 4 shows the formation process of exit edge defects when the tool approaches the end of the workpiece. Fig. 4a shows the initial contact stage between the chip and tool when the tool cut

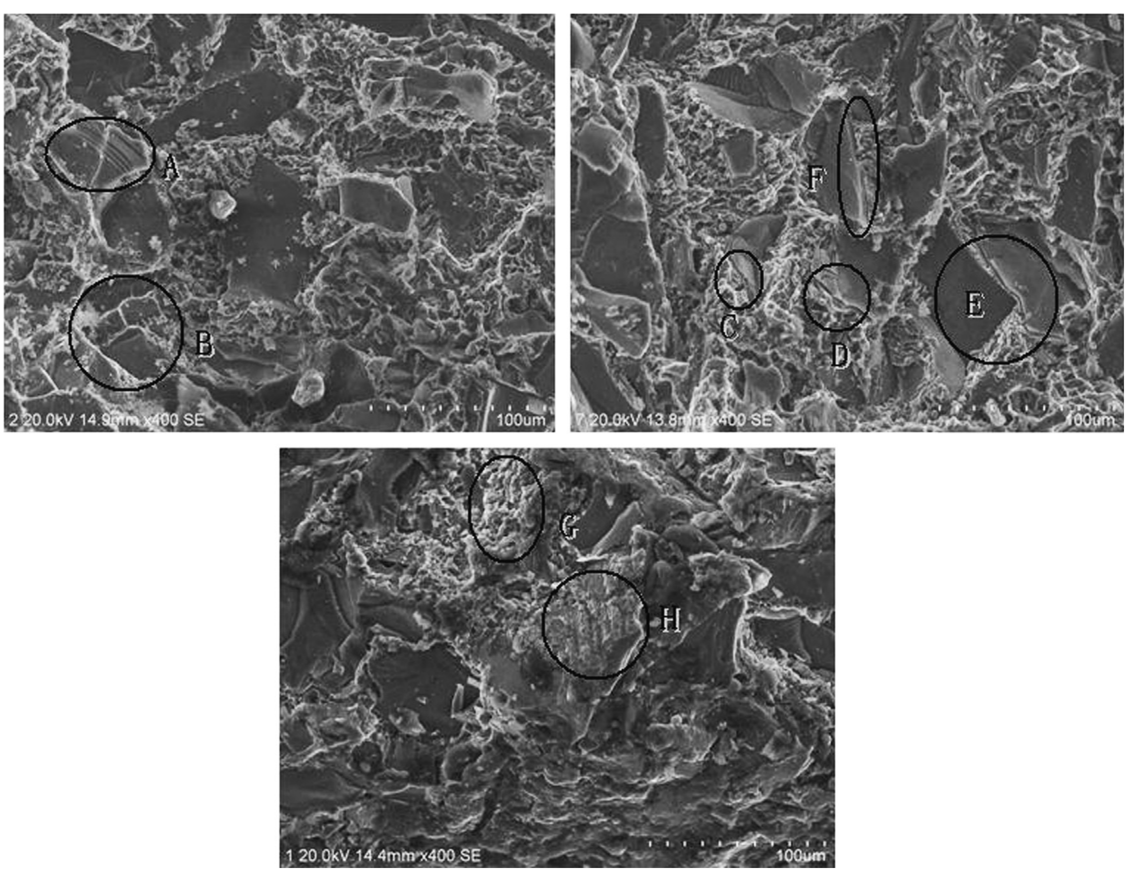

Fig. 5. SEM fractographs of SiCp/Al composites, (a) particle fracture, (b) interface debond and (c) matrix failure.

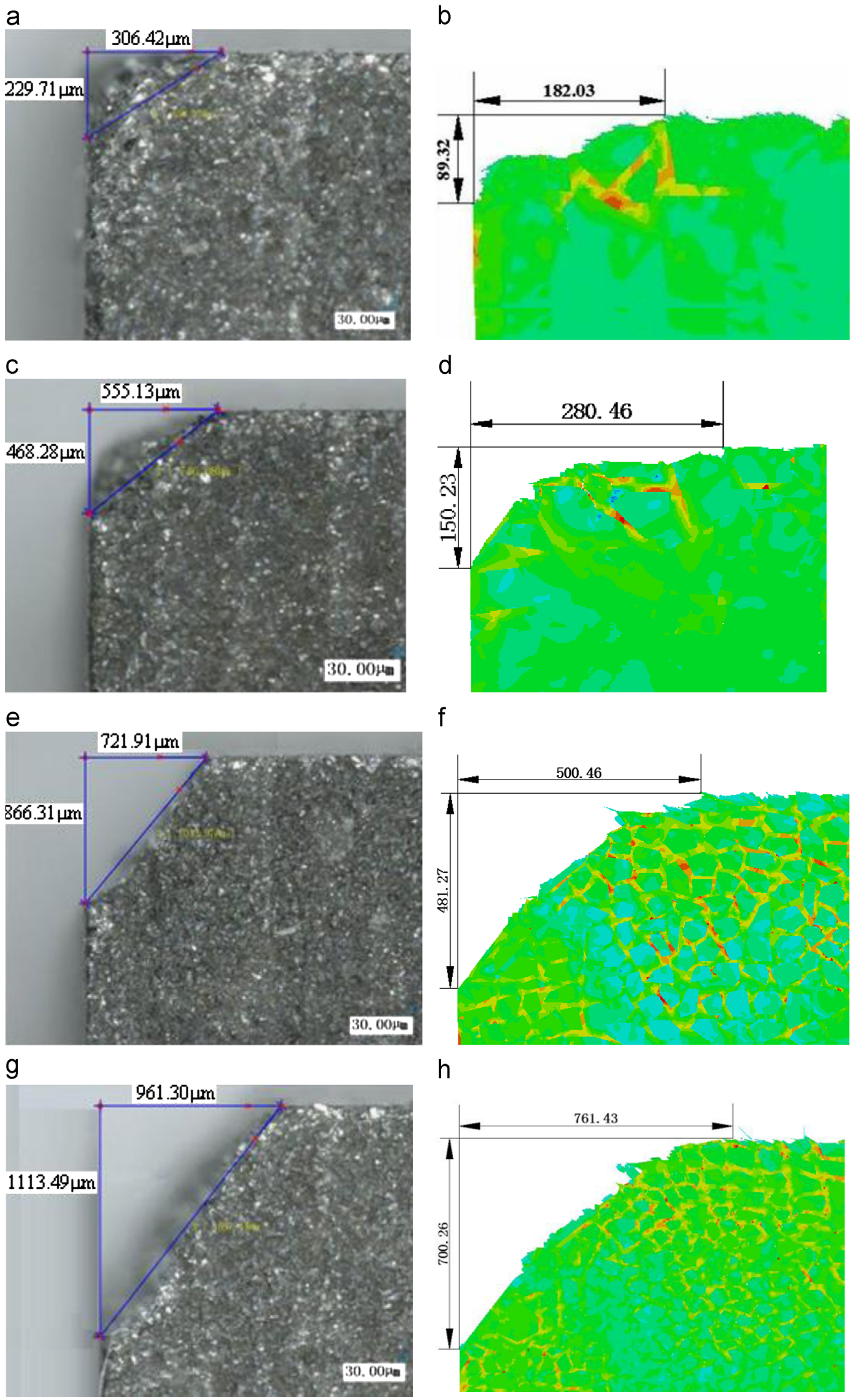

Fig. 6. Edge morphology on the exit surface, at cutting speed of 5 m/min rake angle of 0°, and cutting depth of (a) and (b) ap=0.05 mm, (c) and (d) ap=0.1 mm, (e) and (f) ap=0.15 mm, (g) and (h) ap=0.2 mm.

into workpiece, and the magnitude of equivalent stress reveals that the three basic deformation zones is not obvious, which is very different from that of the homogeneous material. In the first deformation zone, the maximum von Mises equivalent stress is distributed in the aluminum alloy matrix near the SiC particles. Fig. 4b shows the chip formation, in this stage, due to the plastic deformation of Al alloy matrix and SiC particles elastic failure, the crack initiated and the stress released in the primary shear zone. Fig. 4c shows the continuous cutting state. Because of the high volume fraction and large SiC particles in SiCp/Al composites, the brittle failure becomes more prominent and segmented chips are formed. From the figure, it can also be observed that the elastic deformation zone has extended to the edge of the workpiece in this stage. Fig. 4d shows the pivoting stage. The left corner region of the workpiece starts rotating while essentially remaining undeformed. At the same time, it can be noted that the plastic deformation zone around the primary shear zone has extended to the workpiece edge and the negative shear angle begins to form. As the tool moves toward the workpiece edge, the crack initiates and propagates along the negative shear angle, as shown in Fig. 4e and f. From the figures, it can be seen that the deformation of SiCp/Al composites is very different from that of ductile material due to the addition of SiC ceramic particles, and the cracks are presented not only in the Al matrix but also in SiC particles. Fig.4g shows eventually the tool cuts through the workpiece and the edge defects is formed. In this stage, the crack causes separation of the chip along with the part of the workpiece above the negative shear line. As a result, an area consisting of the fractured surface and a small amount of deformed material remains on the workpiece edge and the edge defects is produced.

Fig. 5 gives the fracture surface of edge defects. Brittle fracture of the SiC particles is present and some facets were found in the larger SiC particle, as shown in Fig. 5a. In addition, debonded interface (see Fig. 5b) and ductile failed of the Al matrix (see Fig. 5c) can be also observed. From the fractographs, it can be observed that the fracture surfaces were smoother, and ductile dimples were difficult to observe. So it can be concluded that during machining of SiCp/Al composites with higher volume fraction and larger SiC particle, the brittle fracture mode corresponds to the dominant failure mode.

4.2. Effect of cutting parameters

Fig. 6 shows the experimental and simulated exit edge defects morphology in orthogonal cutting SiCp/Al composites under four different cutting depths. From the experimental results it can be observed that brittle fractures are very clear and the fracture surface is very rough due to the high volume fraction of SiC particle in the composites. With the increase of the cutting depth, the sizes, both the height and width of exit edge defects increase significantly.

The influence of cutting depth on edge defects height and width for experimental and simulation are plotted in Fig. 7a. It is clear that the edge defects height and width increase as the cutting depth increases, and the dependence of edge defects sizes on cutting depth appeared to be linear relationship. The reason is that with the increasing of cutting depth, the higher cutting force will induce the cutting action tends to be more unstable during machining, which increases the exit edge defects size. In addition to cutting depth, the cutting speed is another important parameter during orthogonal cutting. Fig. 7b presents the effect of cutting speed on the sizes of edge defects generated during cutting SiCp/Al composites both for experiment and calculation, and it can be seen that the cutting speed has a very small effect on sizes of edge defects. In this study, due to the limit of machining machine, a lower range of cutting speed was used. On the other hand, due to the low volume fraction of Al matrix, the effect of Al alloy matrix softening is not obviously with increasing cutting speed.

From Fig. 7, it is worth noting that there are some similar phenomena in Fig. 7a and b; the simulated curves (dashed curves) are smoother than the experimental curves (solid curves), and the simulated values are smaller than the experimental values. These can be explained by the present simulation model. In this model, the material is assumed to have no defects and the interface between the Al matrix and the SiC particles need not be considered. In fact, besides many microscopic material defects such as cracks, dislocations, or pore, the tool wear and machine vibration could cause the larger edge defects size obtained from the experiments than that in the calculation. In addition, the micro-cracks or damages are most likely to initiate at the interface between the matrix and particles during cutting experiments, thus, the fact of not taking into account a weak interface between the matrix and the particles also caused the larger edge defects size obtained from the experiments. Moreover, the dislocation pile can result in the concentrated stress. Therefore, in order obtain a fine edge quality and precise machining accuracy, a smaller cutting depth must be used in machining of SiCp/Al composites; on the contrary, the cutting speed can be adopted as high as possible.

5. Conclusions

A microfinite element model and orthogonal cutting experiment were carried out to study the formation mechanism of edge

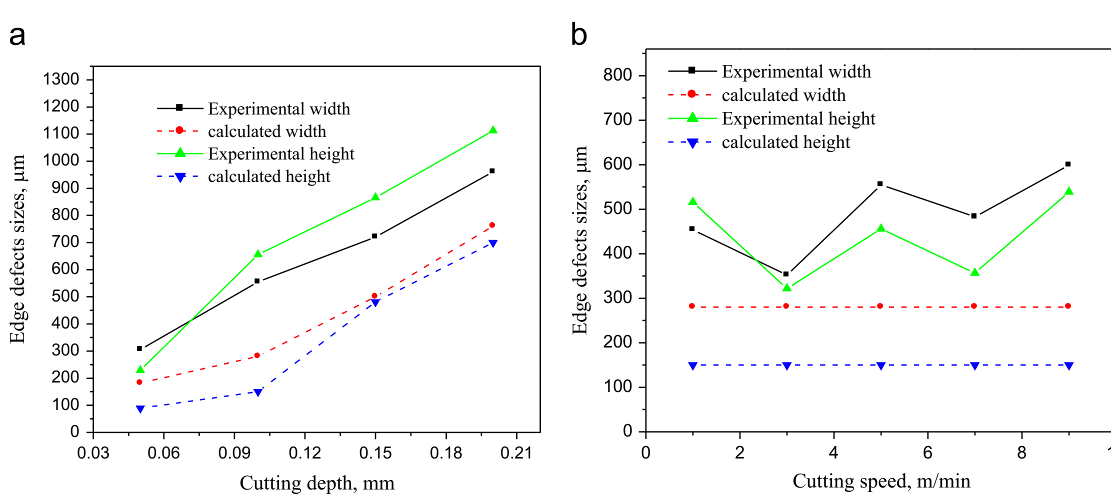

Fig. 7. Influence of cutting parameters on edge defects sizes, (a) cutting depth and (b) cutting speed.

defects and the effects of the cutting parameters on sizes of edge defects during machining of SiCp/Al composites with PCD tools. Good agreement of the results was found between the experimental and calculated. The following conclusions can be drawn:

(1) By using constitutive equations and failure models particular to SiC particles and aluminum alloy matrix, the simulation was successful in predicting the edge defects during machining of SiCp/Al composites. The calculated results show that the edge defects formation can be divided into seven stages: initial contact stage, chip formation, continuous cutting state, formation of negative shear angle, crack initiation, crack propagation and edge defects formation. In addition, the brittle failure becomes more prominent and segmented chips are formed due to the high volume fraction of SiC particles in the composites.

(2) From the experiment and calculation results, it can be concluded that the edge defects size almost linearly increases with increasing cutting depth, while cutting speed has little effect on the sizes of edge defects. Therefore, in precision/superprecision cutting of SiCp/Al composites, cutting speed should be as high as possible, but the cutting depth should be shallow.

Acknowledgments

The authors gratefully acknowledge the financially support by the National Natural Science Foundation of China (51175353).

References

[1] R.D. Chinmaya, C.S. Yung, Modeling of machining of composite materials: a review, Int. J. Mach. Tools Manuf. 57 (2012) 102–121.
[2] G. Tosun, M. Muratoglu, The drilling of an Al/SiCp metal–matrix composites. Part I: microstructure, Compos. Sci. Technol. 64 (2004) 299–308.
[3] A.D. Uday, S.J. Suhas, R. Balasubramaniam, V.V. Bhanuprasad, Surface finish and integrity of machined surfaces on Al/SiCp composites, J. Mater. Process. Technol. 192-193 (2007) 166–174.
[4] R.D. Chinmaya, C.S. Yung, Multi-step 3-D finite element modeling of subsurface damage in machining particulate reinforced metal matrix composites, Composites Part A 40 (2009) 1231–1239.
[5] G.L. Chern, Study on mechanisms of burr formation and edge breakout near the exit of orthogonal cutting, J. Mater. Process. Technol. 176 (2006) 152–157.
[6] A. Toropov, S.L. Ko, B.K. Kim, Experimental study of burrs formed in feed direction when turning aluminum alloy Al6061-T6, Int. J. Mach. Tools Manuf. 45 (2005) 1015–1022.
[7] A. Toropov, S.L. Ko, A model of burr formation in the feed direction in turning, Int. J. Mach. Tools Manuf. 46 (2006) 1913–1920.
[8] J.C. Aurich, D. Dornfeld, P.J. Arrazola, V. Franke, L. Leitz, S. Min, Burrs—analysis, control and removal, CIRP Ann. Manuf. Technol. 58 (2009) 519–542.
[9] G.L. Chern, Experimental observation and analysis of burr formation mechanisms in face milling of aluminum alloys, Int. J. Mach. Tools Manuf. 46 (2006) 1517–1525.
[10] O. Olvera, G. Barrow, An experimental study of burr formation in square shoulder face milling, Int. J. Mach. Tools Manuf. 36 (1996) 1005–1020.
[11] I. Shyha, S.L. Soo, D. Aspinwall, S. Bradley, Effect of laminate configuration and feed rate on cutting performance when drilling holes in carbon fibre reinforced plastic composites, J. Mater. Process. Technol. 210 (2010) 1023–1034.
[12] L.K. Lauderbaugh, Analysis of the effects of process parameters on exit burrs in drilling using a combined simulation and experimental approach, J. Mater. Process. Technol. 209 (2009) 1909–1919.
[13] T.J. Grilo, R.M.F. Paulo, C.R.M. Silva, J.P. Davim, Experimental delamination analyses of CFRPs using different drill geometries, Composites Part B 45 (2013) 1344–1350.
[14] S.S.F. Chang, G.M. Bone, Burr size reduction in drilling by ultrasonic assistance, Robot. Comput. Integr. Manuf. 21 (2005) 442–450.
[15] K. Egashira, Y. Nomura, Y. Murozaki, J. Fukui, Edge finishing and deburring of back surfaces of microholes using micro-cutting tools, Precis. Eng. 37 (2013) 248–254.
[16] T.K. Brockbank, Thermal energy deburring, in: Proceedings of 7th International Conference on Deburring and Surface Finishing, UC Berkeley, CA, 2004, pp. 225–230.
[17] I.H. Choi, J.D. Kim, A study of the characteristics of the electrochemical deburring of a governor-shaft cross hole, J. Mater. Process. Technol. 75 (1998) 198–203.
[18] H. Scheinm, Automatic electrochemical deburring, Soc. Manuf. Eng. 154 (1987) 1–11.
[19] C.X. Ma, E. Shamoto, T. Moriwaki, Y.H. Zhang, L.J. Wang, Suppression of burrs in turning with ultrasonic elliptical vibration cutting, Int. J. Mach. Tools Manuf. 45 (2005) 1295–1300.
[20] B. Yang, X. Shen, S. Lei, Mechanisms of edge chipping in laser-assisted milling of silicon nitride ceramics, Int. J. Mach. Tools Manuf. 49 (2009) 344–350.
[21] W.C. Chiu, M.D. Thouless, W.J. Endres, An analysis of chipping in brittle materials, Int. J. Fract. 90 (1998) 287–298.
[22] Z.C. Li, L.W. Cai, Z.J. Pei, C. Treadwell, Edge-chipping reduction in rotary ultrasonic machining of ceramics: finite element analysis and experimental verification, Int. J. Mach. Tools Manuf. 46 (2006) 1469–1477.
[23] H. Shin, B.M. Song, A method to quantify the drilling machinability of machinable ceramics from the viewpoint of preventing chipping, Ceram. Int. 39 (2013) 9815–9818.
[24] I.W. Park, D.A. Dornfeld, A study of burr formation processes using the finite elements method. Part I., J. Eng. Mater. Technol.—Trans. ASME 122 (2000) 221–229.
[25] I.W. Park, D.A. Dornfeld, A Study of burr formation processes using the finite elements method. Part II. The influences of exit angle, rake angle, and backup material on burr formation processes, J. Eng. Mater. Technol.—Trans. ASME 122 (2000) 229–238.
[26] Y.Q. Cao, Failure analysis of exit edges in ceramic machining using finite element analysis, Eng. Fail. Anal. 8 (2001) 325–338.
[27] Y.B. Guo, D.A. Dornfeld, Finite element analysis of drilling burr minimization with a backup material, Trans. North Am. Manuf. Res. Inst. 207 (1998) 207–211.
[28] V.N. Gaitonde, S.R. Karnik, J.C. Rubio, A.E. Correia, A.M. Abrão, J.P. Davim, Analysis of parametric influence on delamination in high-speed drilling of carbon fiber reinforced plastic composites, J. Mater. Process. Technol. 203 (2008) 431–438.
[29] O. Isbilir, E. Ghassemieh, Numerical investigation of the effects of drill geometry on drilling induced delamination of carbon fiber reinforced composites, Compos. Struct. 105 (2013) 126–133.
[30] J. Zahr Viñuela, J.L. Pérez Castellanos, Elastic constants and isotropy considerations for particulate metal–matrix composites. A multi-particle, cell-based approach, Composites: Part A 42 (2011) 521–533.
[31] Y. Zhu, H.A. Kishawy, Influence of alumina particles on the mechanics of machining metal matrix composites, Int. J. Mach. Tools Manuf. 45 (2005) 389–398.
[32] Y.Q. Tan, D.M. Yang, Y. Sheng, Discrete element method (DEM) modeling of fracture and damage in the machining process of polycrystalline SiC, J. Eur. Ceram. Soc. 29 (2009) 1029–1037.